Proceedings of the
Annual Stability Conference
Structural Stability Research Council
St. Louis, Missouri, April 2-5, 2019

Design by Advanced Elastic Analysis - an investigation of beam-columns resisting minor-axis bending

Yunfei (Phoebe) Wang[1], Ronald D. Ziemian[2]

Abstract
Established methods for system stability design that appear in the American Institute of Steel Construction's *Specification for Structural Steel Buildings* (ANSI/AISC 360-16) include the Direct Analysis Method and the Effective Length Method. Both approaches require the use of the unbraced length of compression members. In 2016, AISC provided an alternate stability design method, Design by Advanced Elastic Analysis, which simplifies current design processes for systems when the unbraced lengths of compressive members are not clearly apparent (e.g. arch). Essential to this approach is the use of an equilibrium analysis that is based on the deformed geometry of the system. With this, the compressive strength of the member may be taken as its cross-section strength; thereby removing any reliance of design equations on the compressive unbraced length of the member. In establishing this approach, many systems were investigated and systems with beam-columns subject to minor-axis bending appeared to deserve additional attention. This paper presents a detailed study that investigates such members. Employing results from advanced inelastic analyses as a basis for comparison, the accuracy of the conventional design methods and this new approach are established. The impact of residual stresses and subjecting the member to major-axis bending instead is also explored. Interaction equation curves for all methods are plotted and radial percent errors are calculated. W-sections over a wide range of member slenderness ratios are investigated. All three design elastic methods provide fairly similar results, with the Design by Advanced Elastic Analysis method providing the largest, but perhaps still considered acceptable, percent errors.

1. Introduction

For the past sixty years, the Effective Length Method (ELM) has been a widely employed stability design method (Ziemian, 2010). By scaling actual unbraced lengths to effective lengths when calculating the available strengths of compression members, the effective length K-factor is assumed to account for most factors known to impact the stability of structural systems, including geometric system imperfections, stiffness reduction due to inelasticity, and to a much lesser degree uncertainty in strength and stiffness (AISC, 2016). In 2005, design by the Direct Analysis Method (DM) first appeared in the American Institute of Steel Construction's (AISC's) *Specification for Structural Steel Buildings*. In DM, the available strengths of compression members are based simply on the unbraced length (K = 1), as long as system imperfections (but not member imperfections) and stiffness reduction due to inelasticity are represented in the structural analysis.

[1] Graduate Student, Cornell University, <yw2252@cornell.edu>
[2] Professor, Bucknell University, <ziemian@bucknell.edu>

Since then, many in the structural design profession have moved from employing ELM to DM. As a result, DM was relocated AISC's 2010 Specification from Appendix 7 to Chapter C, while ELM was relocated from Chapter C to Appendix 7.

Both design methods rely on establishing the unbraced lengths of compression members, which in some cases may be difficult, if not impossible, to define. Examples include, but are not limited to arches, tree columns, and Vierendeel trusses. In response to this predicament, AISC introduced a Design by Advanced Elastic Analysis method that appears in Appendix 1 of their 2016 Specification. In addition to the analysis modeling requirements of DM, the method further requires the direct modeling of member imperfections and, therefore the method is often represented by the acronym DMMI. In applying this approach, engineers can avoid the complexities of defining unbraced lengths, thereby being permitted to compute the strengths of compression members as their axial cross-sectional strengths. This paper reports on an ongoing study to complement previous studies on systems (Nwe Nwe, 2014; Giesen-Loo, 2016) to evaluate the performance of DMMI, especially with an eye towards members that are subject to the combination of compression and minor-axis bending. Using AISC's Design by Advanced Inelastic Analysis Method, which is based on employing a rigorous geometric and material nonlinear analysis with imperfections (GMNIA), the accuracy of DMMI is assessed and further compared with the more traditional ELM and DM design methods. Additionally, the significances of thermal residual stresses, which are a consequence of uneven cooling of rolled cross-sections, and the axis of bending (minor versus major) are also explored.

The paper begins by providing an overview of ELM, DM, and DMMI, along with details of the analysis method and interaction equation employed in each. Results of the study are then presented primarily in tabular format, which are followed by discussions of the effects residual stresses, axis of bending, and design method employed.

2. Overview of Design Methods

In this study, the ends of simply supported columns of various slenderness ratios are subjected to a wide range of combinations of applied axial force and end bending moments that are of equal magnitude and opposite direction (in the absence of axial force such moments would produce a uniform moment distribution). In all cases, the members are assumed to be fully braced out-of-the-plane of bending. To assess the LRFD strength of beam-columns based on an elastic analysis, the following interaction equation is provided in AISC's Specification:

For $P_u/\phi P_n \geq 0.2$,

$$\frac{P_u}{\phi P_n} + \frac{8}{9}\left(\frac{M_{ux}}{\phi M_{nx}} + \frac{M_{uy}}{\phi M_{ny}}\right) \leq 1.0 \quad (1)$$

For $P_u/\emptyset P_n < 0.2$,

$$\frac{P_u}{2\phi P_n} + \left(\frac{M_{ux}}{\phi M_{nx}} + \frac{M_{uy}}{\phi M_{ny}}\right) \leq 1.0 \quad (2)$$

where P_u is the required axial strength, M_u is the required bending strength, P_n is the nominal axial strength, and M_n is the nominal bending moment about either the major *x*- or minor *y*-axis. The analysis for the required axial strength P_u and flexural strength M_u should include second-order (geometric nonlinear) effects.

The following design methods, including ELM, DM, and DMMI, are represented by Eq. 1 with terms defined per that specific method. In all cases, the controlling combinations of axial force and bending moment are determined for each of these elastic design methods by iteratively solving for the maximum value of M_u for a given value of P_u that will satisfy Eq. 1.

2.1 Effective Length Method (ELM)

In computing the nominal axial strength P_n from AISC's column curve, the effective length factor of a simply supported beam-column is $K = 1$. In determining the required flexural strength M_u, equilibrium equations are defined on the deflected shape to account for second-order effects. For a structural analysis associated with ELM, the beam-column is assumed geometrically straight prior to any applied loading (AISC's column curve accounts for member out-of-straightness). As a result, the $P - \delta$ effect in this method accounts only for the interaction between the applied axial load and bending moments, and thereby is not influenced by the presence of an initial member imperfection. Fig. 1 shows the deflected shape of the beam-column, in which $v_{PM}(x)$ is the elastic curve of the deformed shape as a result of applied end actions that include axial force P and bending moment M.

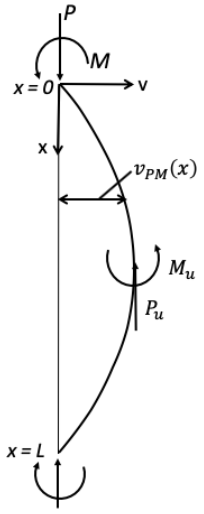

Figure 1: Deflected shape of beam-columns with second-order effects included

At any point along the span of the member, equilibrium on the deformed shape requires:

$$M_u(x, P) + P \cdot v_{PM}(x) + M = 0 \tag{3}$$

In establishing the design adequacy of this member, the required moment $M_u(x, P)$ is a maximum at mid-span because $v_{PM}(x)$ takes on a maximum value when $x = L/2$. Thus, the interaction equation only needs to be checked at mid-span, where the required strengths (terms in the numerators) are at a peak. For an elastic analysis of a simply supported, originally perfectly straight, and prismatic member, the deflection and required flexural strength M_u at mid-span, which includes second-order effects, can be calculated as a function of the applied force P and moment M by the following "exact" equation (McGuire et al., 2000):

$$\left|M_{u\_mid}\right| = \frac{1}{\cos\left(\frac{\pi}{2}\sqrt{P/P_e}\right)} M \tag{4}$$

where P_e = Euler buckling strength of the beam-column.

With $P_u = P$ at mid-span, substitution of these terms for P_u and $M_u = \left|M_{u\_mid}\right|$ in Eq. 1 results in an interaction equation for ELM defined by:

$$\frac{P}{\phi P_n} + \frac{8}{9} \cdot \frac{\frac{1}{\cos\left(\frac{\pi}{2}\sqrt{P/P_e}\right)} M}{\phi M_n} \leq 1.0 \tag{5}$$

In which specific to ELM,

$P_n = F_{cr} A_g$

$P_e = \pi^2 EI/L^2$

$M_n = F_y \mathrm{Z}$

where, F_{cr} is the critical buckling stress as defined by AISC's column curve with K = 1 for the simply supported end conditions being investigated in this study, A_g is the gross area of the cross-section, E is the elastic modulus of the material, I is the moment of inertia, L is the unsupported length of the beam-column, F_y is the material yield stress, and Z is the plastic section modulus. In computing M_n, it is important to note that only members with compact sections are investigated, and any members subject to major-axis bending are assumed fully braced out-of-plane.

2.2 Direct Analysis Method (DM)

Although DM permits the use of the unbraced length (K = 1), this provides no advantage over ELM for the specific end support conditions of the single beam-column investigated in this study. In fact, DM is somewhat penalized in this case by its required use of a stiffness reduction factor within the structural analysis. Although the equilibrium analysis is of the same form as that given for ELM, the Euler buckling strength P_e of the member is modified to represent the inelastic buckling strength of the member. As a result, interaction equation Eq. 1 for DM can be rewritten as Eq. 5, similar to that for ELM. However, P_e in Eq. 5 is specified differently. In summary, Eq. 5 applies for DM with:

$P_n = F_{cr} A_g$, with F_{cr} defined by AISC's column curve with no $0.8\tau_b$ stiffness reduction on E

$P_e = \pi^2 (0.8\tau_b E)\mathrm{I}/L^2$

$M_n = F_y \mathrm{Z}$

According to the AISC Specification (2016) and given that all sections are compact, τ_b is calculated as

$\tau_b = 4(P/P_y)[1 - (P/P_y)]$ for $P/P_y > 0.5$, and $\tau_b = 1.0$ for $P/P_y \leq 0.5$

where $P_y = F_y A_g$.

2.3 Design by Advanced Elastic Analysis Method (DMMI)

As described earlier, DMMI is an alternative design method that may be particularly useful for more complex structures in which the unbraced length is not discernable. By directly modeling member out-of-straightness and representing potential inelasticity through the use of stiffness

reduction strategy employed in DM, the design axial strength P_n of the member may be taken as its cross-section strength. The artificial and dramatic increase in axial strength P_n that appears in the interaction equation is compensated for by larger required flexural strength M_u, which is obtained from an advanced elastic structural analysis that accounts for initial system and member imperfections, second-order (geometric nonlinear) effects, and stiffness reduction due to inelasticity.

In contrast to the above analysis for determining strengths for ELM and DM, the analysis for DMMI must also include the direct modeling of member out-of-straightness. In this study, the shape of the initial imperfection is assumed a sine wave with an amplitude at mid-span of $L/1000$ per the AISC's *Code of Standard Practice for Steel Buildings and Bridges* (AISC, 2016a). As such, the second-order $P-\delta$ effect needs to include both the impact of the applied axial force and bending moment as well as the initial imperfection. Fig. 2 shows the initial imperfection $v_0(x)$ and final deflected shape $v(x)$ due to combined effect of the applied loading and geometric imperfection.

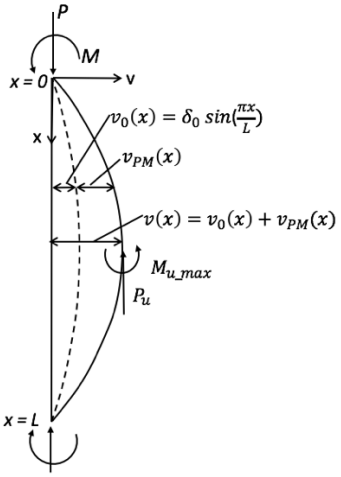

Figure 2: Deflected shape of beam-column with second-order effects due to applied loading and geometric imperfection

In this case, equilibrium on the deformed shape is given by:

$$M_u(x,P) + P \cdot v(x) + M = 0 \tag{6}$$

where $v(x)$ is the total lateral deflection as a function of span length location x, which equals the sum of geometric imperfection, $v_0(x) = \delta_0 \cdot \sin(\frac{\pi x}{L})$, and deflection $v_{PM}(x)$ due to the applied combination of P and M. Starting with an elastic moment-curvature relationship, the moment equilibrium equation can be rewritten as:

$$EI\frac{d^2 v_{PM}}{dx^2} + P v_{PM}(x) + P v_0(x) + M = 0 \tag{7}$$

The solution to this differential equation is:

$$v_{PM}(x) = \frac{\delta_0 \cdot \sin\left(\frac{\pi x}{L}\right)}{\frac{P_e}{P} - 1} + \frac{M}{P} \cdot \frac{\sin\left(\sqrt{\frac{P}{EI}}x\right) - \cos\left(\sqrt{\frac{P}{P_e}}\pi\right) \cdot \sin\left(\sqrt{\frac{P}{EI}}x\right) - \sin\left(\sqrt{\frac{P}{P_e}}\pi\right) + \cos\left(\sqrt{\frac{P}{EI}}x\right) \cdot \sin\left(\sqrt{\frac{P}{P_e}}\pi\right)}{\sin\left(\sqrt{\frac{P}{P_e}}\pi\right)} \quad (8)$$

As a result, the total deflection $v(x)$, which is the sum of $v_{PM}(x)$ and $v_0(x)$, is expressed as:

$$v(x) = \frac{\delta_0 \cdot \sin\left(\frac{\pi x}{L}\right)}{1 - \frac{P}{P_e}} + \frac{M}{P} \cdot \frac{\sin\left(\sqrt{\frac{P}{EI}}x\right) - \cos\left(\sqrt{\frac{P}{P_e}}\pi\right) \cdot \sin\left(\sqrt{\frac{P}{EI}}x\right) - \sin\left(\sqrt{\frac{P}{P_e}}\pi\right) + \cos\left(\sqrt{\frac{P}{EI}}x\right) \cdot \sin\left(\sqrt{\frac{P}{P_e}}\pi\right)}{\sin\left(\sqrt{\frac{P}{P_e}}\pi\right)} \quad (9)$$

Given that the mid-span $x = L/2$ remains the critical location to check for stability, the total deflection can be expressed as:

$$v\left(\frac{L}{2}\right) = \frac{\delta_0}{1 - \frac{P}{P_e}} + \frac{M}{P} \cdot \frac{\sin\left(\sqrt{\frac{P}{P_e}}\frac{\pi}{2}\right) - \cos\left(\sqrt{\frac{P}{P_e}}\pi\right) \cdot \sin\left(\sqrt{\frac{P}{P_e}}\frac{\pi}{2}\right) - \sin\left(\sqrt{\frac{P}{P_e}}\pi\right) + \cos\left(\sqrt{\frac{P}{P_e}}\frac{\pi}{2}\right) \cdot \sin\left(\sqrt{\frac{P}{P_e}}\pi\right)}{\sin\left(\sqrt{\frac{P}{P_e}}\pi\right)} \quad (10)$$

With $v\left(\frac{L}{2}\right)$, equilibrium on the deformed shape at mid-span will result in a required moment strength of:

$$\left|M_{u\_mid}\right| = M + P \cdot v\left(\frac{L}{2}\right) \quad (11)$$

Similar to DM, a stiffness reduction factor of $0.8\tau_b$ should be applied to all the members of the system, which in this study means that all *EI* terms (within P_e) in the above equations should be $0.8\tau_b EI$. With values of $P_u = P$ and $M_u = \left|M_{u\_mid}\right|$ as defined above, the interaction equation Eq. 1 is expressed for DMMI as:

$$\frac{P}{\phi P_n} + \frac{8}{9} \cdot \frac{M + P \cdot v\left(\frac{L}{2}\right)}{\phi M_n} \leq 1.0 \quad (12)$$

In which specific to DMMI,

$v\left(\frac{L}{2}\right)$ is given by Eq. 10, with $\delta_0 = L/1000$, and P_e and τ_b as defined for DM

$P_n = F_y A_g$ and $M_n = F_y Z$

2.4 Design by Advanced Inelastic Analysis Method (GMNIA)

Since 2010, the Design by Advanced Inelastic Analysis Method has been provided in Appendix 1 of the AISC Specification. Given that this design method is based on a geometric and materially nonlinear analysis, it will be referenced by the acronym GMNIA. The second-order inelastic analysis routines used in this study are included in the finite element analysis software FE++ (Alemdar, 2001), in which a distributed plasticity model is employed. Each beam-column is modeled by eight line elements, thereby permitting a sine wave member out-of-straightness of $\delta_0 = L/1000$ to be directly modeled in the analysis. Residual stresses are represented by pre-stressing (compression or tension) the cross-section fibers that define the cross-section. The

applied axial force P and bending moments M are applied simultaneously, and an incremental-iterative arc length solution scheme is employed until a limit point is achieved. Because of the relatively high accuracy of this analysis, an error analysis of the above elastic design methods is based on the combinations of P and M that this inelastic design method would permit and still satisfy the provisions of Appendix 1 of AISC's Specification.

It is well known that partial yielding of the cross-section can have a significant effect on the stability of beam-columns. In cases where member imperfections are not removed by processes, such as rotary straightening, this partial yielding can be accentuated by the presence of residual stresses. On the other hand, the use of such straightening processes can be shown to alleviate or even eliminate the presence of residual stresses (Ge and Yura, 2019). As result, ultimate strength combinations were determined for cases in which residual stresses were and were not included in the analysis. When residual stresses are taken into account, the Galambos and Ketter (1959) residual stress distribution shown in Fig. 3 was employed with a maximum compressive stress at the flange tips of $0.3F_y$. Additionally, the material elastic modulus E and yield stress F_y are reduced by a factor of 0.9, per the requirements of Appendix 1 of the AISC Specification. An elastic-perfectly plastic material model is employed.

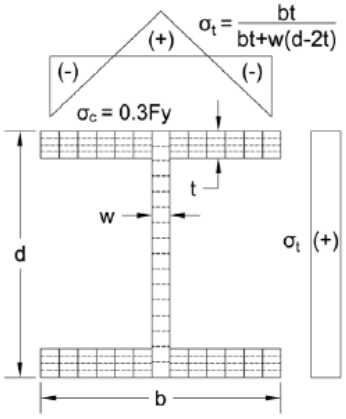

Figure 3: Residual stress distribution of Galambos and Ketter (1959)

3. Normalized *P-M* Interaction Curves and Error Calculation

To compare the accuracy of each of the design methods, with special attention on DMMI, normalized *P-M* interaction curves of ELM, DM, DMMI, and GMNIA are first plotted. Data points are obtained by determining the maximum combination of axial load P and bending moments M that can be applied at the member ends such that the strength requirements of the design method would just be satisfied. Calculation of error values in the curves are then computed using the GMNIA curve as a basis. To further allow the errors to be comparable for the wide range of member slenderness ratios investigated, all axial forces and moments were normalized by the maximum GMNIA values, with P^{GMNIA} being the maximum axial strength when the applied moment is $M = 0$, and with M^{GMNIA} being the maximum moment strength when the applied axial force is $P = 0$ (which would equal $0.9F_yZ$ for all members in this study). As an example, Figure 4 shows the normalized *P-M* interaction curves and a plot of the radial errors for a W12X50 member with an $L/r = 90$ that is subjected to minor-axis bending and with residual stresses included. Plots for the same member and conditions of the four other L/r slenderness ratios (30, 60, 120, and 150) studied are provided in Appendix A.

Using radial lines at 10° increments measured clockwise from the normalized P-axis to the M-axis, the intersections of the radial lines and the P-M curves are found. It is noted that values at intersection points that lay between data points are obtained from a parabolic interpolation between the adjacent three data points. The percent errors of the design methods are then established by comparing their radial R-distances from the origin to the interaction curves according to:

$$percent\ radial\ error = \frac{R_{XXX} - R_{GMNIA}}{R_{GMNIA}} \times 100\% \tag{13}$$

where R_{XXX} is the radial distance of the P-M curves for the elastic design methods (ELM, DM, and DMMI), and R_{GMNIA} is radial distance to the GMNIA P-M curve. As a result, error plots (Fig. 4b) at different radial angles represent a comprehensive range of different combinations of applied axial force and moment.

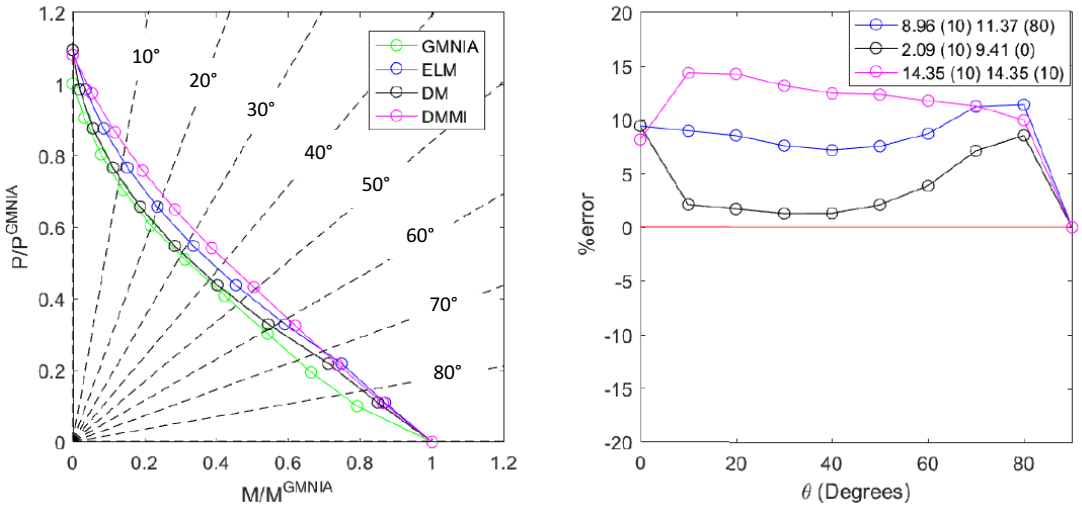

(a) (b)

Figure 4: For a W12X50 member with an L/r = 90 subject to minor-axis bending and with residual stresses included, (a) normalized P-M interaction curves of the four design methods, and (b) plots of percent radial errors

The legend within the radial error graph (Fig. 4b) contains information important to this study. Working from the top downward, rows within this legend represent results for the ELM, DM, and DMMI methods, respectively. The first two numbers in each row represent the error of each design method with an angle (θ) that corresponds to where the DMMI error is at its maximum. The second two numbers correspond to the maximum error of each design method and the angle (θ) where this maximum occurs. Points with positive percent errors are indicative of situations in which the elastic design method (ELM, DM, or DMMI) are unconservative when compared to design strengths determined by GMNIA.

4. Cross-sections investigated

As indicated in Table 1, this study investigated 65 wide flange W-shapes of A992 steel (E = 29,000ksi and F_y = 50ksi). These shapes are all of the compact sections that appear in the column design portion of the AISC Manual (AISC, 2016b), and their depth to width ratios are all less than 1.5.

Table 1: W-shapes studied

W14	W14X730	W14X665	W14X605	W14X550	W14X500	W14X455	W14X426
	W14X398	W14X370	W14X342	W14X311	W14X282	W14X257	W14X233
	W14X211	W14X193	W14X176	W14X159	W14X145	W14X132	W14X120
	W14X109	W14X82	W14X74	W14X68	W14X61	W14X53	W14X48
W12	W12X336	W12X305	W12X279	W12X252	W12X230	W12X210	W12X190
	W12X170	W12X152	W12X136	W12X120	W12X106	W12X96	W12X87
	W12X79	W12X72	W12X58	W12X53	W12X50	W12X45	W12X40
W10	W10X112	W10X100	W10X88	W10X77	W10X68	W10X60	W10X54
	W10X49	W10X45	W10X39	W10X33			
W8	W8X67	W8X58	W8X48	W8X40	W8X35		

5. Results

Interaction curves and plots of percent radial errors that correspond to the four different design methods (ELM, DM, DMMI, and GMNIA) were prepared (see for example, Fig. 4) for all 65 W-shapes over a range of member slenderness L/r ratios of 30, 60 , 90, 120, and 150, with $r = \sqrt{I/A}$. With four cases, including minor- or major-axis bending and with or without residual stresses, this study evaluates 1,300 conditions, which are represented by a total of 57,200 analysis data points. An example of the specific results for a W12x50 member are provided in Appendix B.

A summary of the results for all members are provided in Table 2, in which the maximum, average, and median of all of the individual member maximum percent radial errors are reported. In general, the percent radial errors reported for the three design methods are fairly similar. The largest percent radial errors are always for the DMMI method, and the smallest percent radial errors are for the DM method. Given that the ELM and DM methods are essentially the same, except that DM requires the analysis to include the stiffness reduction $0.8\tau_b$, it is expected (and confirmed in Table 1) that DM will be more conservative (smaller radial errors) than ELM for all slenderness ratios.

As exemplified in Fig. 4, it is further noted that larger unconservative errors for DMMI for sections with residual stresses consistently occur when the applied loading combination is predominately axial force ($\theta = 10°$), where in contrast the larger unconservative errors for ELM and DM occur when the loading is primarily bending ($\theta = 80°$).

Table 2: Summary of percent radial errors

	Minor-axis bending with residual stresses	Minor-axis bending without residual stresses	Major-axis bending with residual stresses	Major-axis bending without residual stresses
$L/r = 30$	DMMI Max= 3.0% Ave= 2.2% Median= 2.2%	DMMI Max= 1.8% Ave= 0.5% Median= 0.4%	DMMI Max= 7.0% Ave= 6.5% Median= 6.6%	DMMI Max= 5.9% Ave= 5.0% Median= 5.0%
	ELM Max= 3.2% Ave= 2.1% Median= 2.0%	ELM Max= 2.5% Ave= 1.1% Median= 1.1%	ELM Max= 6.9% Ave= 6.1% Median= 6.2%	ELM Max= 5.8% Ave= 4.7% Median= 4.6%
	DM Max= 2.6% Ave= 1.5% Median= 1.5%	DM Max= 1.9% Ave= 0.6% Median= 0.5%	DM Max= 6.0% Ave= 5.1% Median= 5.2%	DM Max= 4.9% Ave= 3.8% Median= 3.6%

$L/r = 60$	DMMI Max= 14.8% Ave= 13.7% Median= 13.9%	DMMI Max= 7.3% Ave= 6.1% Median= 6.1%	DMMI Max= 10.5% Ave= 10.0% Median= 10.0%	DMMI Max= 7.5% Ave= 6.7% Median= 6.6%
	ELM Max= 9.7% Ave= 8.4% Median= 8.4%	ELM Max= 8.8% Ave= 7.5% Median= 7.6%	ELM Max= 9.2% Ave= 8.5% Median= 8.6%	ELM Max= 6.1% Ave= 5.2% Median= 5.3%
	DM Max= 8.2% Ave= 7.3% Median= 7.3%	DM Max= 6.7% Ave= 5.5% Median= 5.5%	DM Max= 6.4% Ave= 5.7% Median= 5.8%	DM Max= 3.6% Ave= 2.9% Median= 3.0%
$L/r = 90$	DMMI Max= 15.8% Ave= 14.8% Median= 14.8%	DMMI Max= 9.7% Ave= 8.2% Median= 8.2%	DMMI Max= 10.0% Ave= 9.2% Median= 9.2%	DMMI Max= 5.4% Ave= 4.7% Median= 4.7%
	ELM Max= 13.0% Ave= 11.1% Median= 11.1%	ELM Max= 11.3% Ave= 9.8% Median= 9.8%	ELM Max= 7.6% Ave= 6.9% Median= 6.9%	ELM Max= 4.5% Ave= 3.5% Median= 3.5%
	DM Max= 11.2% Ave= 9.6% Median= 9.6%	DM Max= 8.2% Ave= 6.7% Median= 6.7%	DM Max= 3.9% Ave= 3.2% Median= 3.3%	DM Max= 1.5% Ave= 0.6% Median= 0.6%
$L/r = 120$	DMMI Max= 15.3 % Ave= 14.2% Median= 14.1%	DMMI Max= 11.0% Ave= 9.6% Median= 9.6%	DMMI Max= 7.1% Ave=6.2% Median= 6.2%	DMMI Max= 2.9% Ave= 2.2% Median= 2.2%
	ELM Max= 12.7% Ave= 11.3% Median= 11.3%	ELM Max= 11.4% Ave= 9.9% Median= 9.9%	ELM Max= 5.8% Ave= 4.6% Median= 4.6%	ELM Max= 2.7% Ave= 1.8% Median= 1.8%
	DM Max= 9.5% Ave= 8.0% Median= 8.0%	DM Max= 8.1% Ave= 6.6% Median= 6.6%	DM Max= 2.6% Ave= 1.5% Median= 1.4%	DM* Max= n/a Ave= n/a Median= n/a
$L/r = 150$	DMMI Max= 14.0% Ave= 12.6% Median= 12.6%	DMMI Max= 11.8% Ave= 10.4% Median= 10.4%	DMMI Max= 5.6% Ave= 4.8% Median= 4.7%	DMMI Max= 2.1% Ave= 1.2% Median= 1.2%
	ELM Max= 12.4% Ave= 10.9% Median= 10.9%	ELM Max= 11.2% Ave= 9.8% Median= 9.8%	ELM Max= 4.4% Ave= 3.4% Median= 3.4%	ELM Max= 1.4% Ave= 0.5% Median= 0.5%
	DM Max= 9.0% Ave= 7.6% Median= 7.6%	DM Max= 7.8% Ave= 6.4% Median= 6.4%	DM Max= 1.1% Ave= 0.2% Median= 0.1%	DM* Max= n/a Ave= n/a Median= n/a

DM* no unconservative errors are observed

5.1 Effects of Residual Stresses

As would be expected, not including a residual stress distribution increases the design capacities of the beam-columns per the GMNIA design method. As a consequence, and given that the GMNIA results form the basis for the error analysis, the unconservative percent radial errors for

all three of the elastic design methods (ELM, DM, and DMMI) are significantly reduced. A representative example of this is shown in Fig. 5, where the performance of the DMMI design method is significantly improved with much better agreement (smaller radial errors) with GMNIA. This increase in accuracy, however, is relatively pronounced where θ is small, when the axial load is more significant than the bending moment, and is less obvious when θ is large, a combination of a larger bending moment and a smaller axial force. Of course, this is expected because it is well known that such residual stresses rarely impact the strength of a member primarily subjected to a loading combination that is predominately bending (again noting that all members in this study are either subject to minor-axis bending or laterally braced when subject to major-axis flexure). The trend observed in Fig. 5 is consistent for all shapes and design methods investigated in this study, regardless of the slenderness ratio or the axis of bending investigated. It is further noted that the ELM and DM design methods are significantly more conservative when residual stresses are not present.

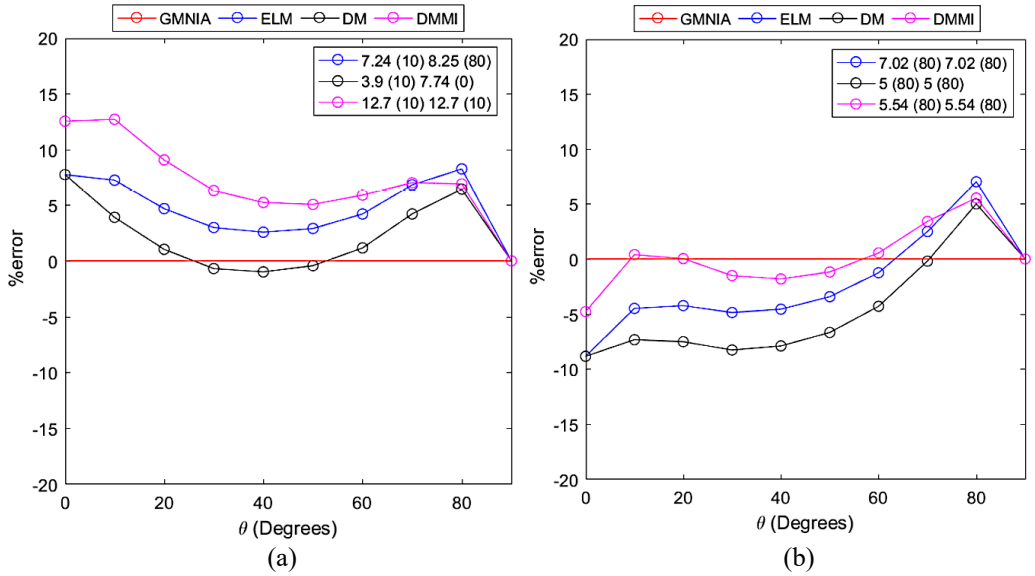

Figure 5: Percent radial errors for a member of an $L/r = 60$ subjected to minor-axis bending comprised of a W12X50 section that (a) includes and (b) excludes residual stresses in the GMNIA-based design

With a focus on the DMMI method, Table 3 shows the maximum and average of the maximum changes in the individual percent radial errors for all 65 W-sections as a result of not including the residual stress effect in the GMNIA-based design. Results for both minor-axis and major-axis bending are provided. All changes reported indicate a reduction in the percent error. For example, the maximum radial error of all members with an $L/r = 60$ subject to minor-axis bending was reduced by $\Delta_{Max} = 8.4\%$ with an average maximum change of $\Delta_{Ave} = 7.7\%$. The reduction in DMMI errors for sections with and without residual stresses is largest when the slenderness ratio is $L/r = 60$ for minor-axis bending and $L/r = 90$ for major-axis bending. The change in error is the smallest at the extreme slenderness ratios investigated, including the least-slender ($L/r = 30$) and most-slender ($L/r = 150$) members.

Table 3: Effect on DMMI results when excluding residual stresses in the GMNIA-based design (reduction in percent radial error)

Slenderness Ratio	Minor-axis bending	Major-axis bending
30	Δ_{Max}= 2.5% Δ_{Ave}= 1.7%	Δ_{Max}= 2.2% Δ_{Ave}= 1.5%
60	Δ_{Max}= 8.4% Δ_{Ave}= 7.7%	Δ_{Max}= 4.1% Δ_{Ave}= 3.3%
90	Δ_{Max}= 7.0% Δ_{Ave}= 6.5%	Δ_{Max}= 5.4% Δ_{Ave}= 4.6%
120	Δ_{Max}= 5.1% Δ_{Ave}= 4.6%	Δ_{Max}= 4.6% Δ_{Ave}= 4.0%
150	Δ_{Max}= 2.6% Δ_{Ave}= 2.3%	Δ_{Max}= 4.0% Δ_{Ave}=3.6%

* Δ_{Max}= maximum of all of the individual maximum changes for the 65 W-sections investigated by DMMI when moving from including residual stresses to excluding residual stresses in the GMNIA-based design.
* Δ_{Ave}= average of all of the individual maximum changes for the 65 W-sections investigated by DMMI when moving from including residual stresses to excluding residual stresses in the GMNIA-based design.

5.2 Effect of Bending Axis

Using an approach similar to that used in the previous section, the DMMI method was investigated with regard to the axis of the bending moment. The example in Fig. 6 is representative of the results observed, in which the percent radial error is significantly reduced when moving from minor-axis bending to major-axis bending, while the slenderness ratio remains the same. Similarly, the change in the DMMI results for all members are provided in Table 4. For the example of $L/r = 90$, changing the bending axis from minor to major for the condition of when residual stresses are excluded produces a reduction in the maximum percent radial error of Δ_{Max} = 5.1% with an average maximum change of Δ_{Ave} = 3.5%. Negative values in Table 4 indicate an increase in the error. With the exception of more-stocky members ($L/r = 30$), the percent radial errors are reduced when members are subject to major-axis flexure instead of minor-axis bending.

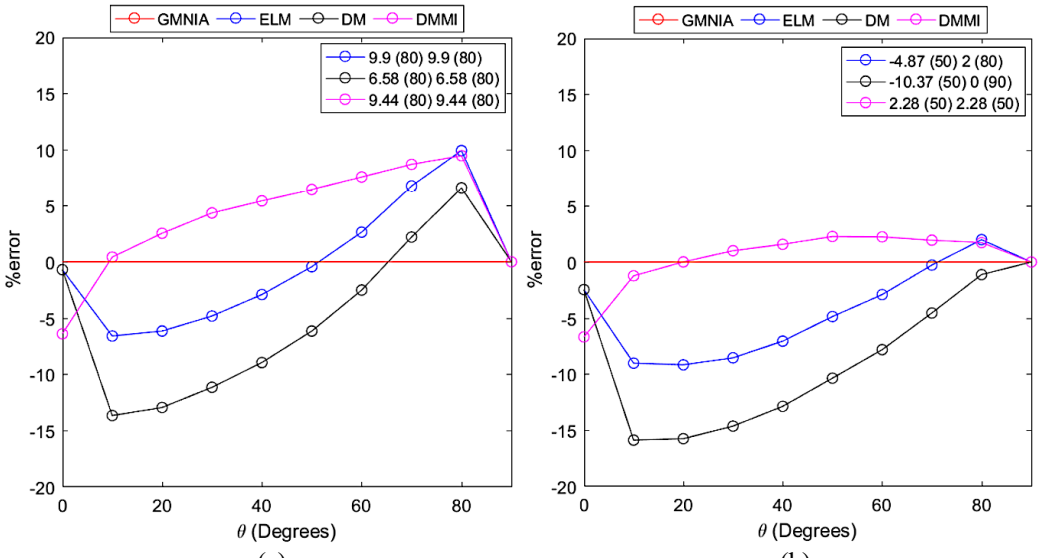

Figure 6: Percent radial errors for members of an $L/r = 120$ with a W12x50 section that excludes residual stresses subjected to (a) minor-axis and (b) major-axis bending

Table 4: Effect of bending axis on DMMI results (reduction in percent radial error)

Slenderness Ratio	Residual stresses included in the GMNIA-based design	Residual stresses excluded in the GMNIA-based design
30	Δ_{Max}= -3.6% Δ_{Ave}= -4.3%	Δ_{Max}= -2.8% Δ_{Ave}= -4.5%
60	Δ_{Max}= 4.9% Δ_{Ave}= 3.7%	Δ_{Max}= 1.0% Δ_{Ave}= -0.6%
90	Δ_{Max}= 6.9% Δ_{Ave}= 5.5%	Δ_{Max}= 5.1% Δ_{Ave}= 3.5%
120	Δ_{Max}= 9.3% Δ_{Ave}= 7.9%	Δ_{Max}= 9.1% Δ_{Ave}= 7.3%
150	Δ_{Max}= 9.4% Δ_{Ave}= 7.9%	Δ_{Max}= 11.1% Δ_{Ave}=9.2%

* Δ_{Max}= maximum of all of the individual maximum changes for the 65 W-sections investigated by DMMI when moving from minor-axis bending to major-axis bending.
* Δ_{Ave}= average of all of the individual maximum changes for the 65 W-sections investigated by DMMI when moving from minor-axis bending to major-axis bending.

5.3 Comparison with ELM and DM

As shown in Table 2, all three elastic design methods will produce unconservative errors when compared with GMNIA-based design. For the reasons given earlier, DM will always provide smaller percent radial errors when compared with ELM. This applies only for the simply-supported member explored in this study – for systems comprised of members with effective length *K*-factors exceeding 1.0, this will not necessarily be the case (Martinez-Garcia, 2006).

Table 5: Summary of effect of changing bending axis

Slenderness Ratio	Minor-axis bending	Major-axis bending
30	Δ_{Max}= 1.3% Δ_{Ave}= 0.1%	Δ_{Max}= 0.6% Δ_{Ave}= 0.4%
60	Δ_{Max}= 5.8% Δ_{Ave}= 5.3%	Δ_{Max}= 2.6% Δ_{Ave}= 1.4%
90	Δ_{Max}= 4.2% Δ_{Ave}= 3.7%	Δ_{Max}= 3.6% Δ_{Ave}= 2.3%
120	Δ_{Max}= 3.4% Δ_{Ave}= 2.9%	Δ_{Max}= 2.2% Δ_{Ave}= 1.6%
150	Δ_{Max}= 1.9% Δ_{Ave}= 1.7%	Δ_{Max}= 1.6% Δ_{Ave}=1.4%

* Δ_{Max}= maximum of all of the individual maximum changes for the 65 W-sections investigated when moving from DMMI to ELM.
* Δ_{Ave}= average of all of the individual maximum changes for the 65 W- sections investigated when moving from DMMI to ELM.

To provide a basis for interpreting the errors observed by DMMI, the maximum and average change in the maximum errors associated with moving from DMMI to ELM are presented in Table 5. For the condition of including residual stresses in the GMNIA-based design, changes are reported for both minor- and major-axis bending. The positive values reported indicate that the percent radial errors are reduced. For example, the maximum observed for the maximums of all members with an L/r = 60 subject to minor-axis bending was a reduction in the error of Δ_{Max} = 5.8%, with the average change in the maximum of all sections being Δ_{Ave} = 5.3%. This indicates that results for DMMI and ELM are not significantly different, with the largest differences

occurring for members subject to minor-axis bending in the low- to mid-slenderness (L/r = 60 to 90). Knowing that ELM has been a well-established design method that has performed well in the U.S. since the early 1960's, it is the authors' opinion that the unconservative errors reported in Table 1 for all three elastic design methods may not be reason for significant concern.

6. Summary and Conclusions

This study evaluates three elastic design methods (ELM, DM, and DMMI) appearing in the 2016 AISC Specification by making comparisons with a forth inelastic method that some may consider the most "exact" and titled Design by Advanced Inelastic Analysis Method, which also appears in this Specification. With 1,300 conditions studied that required a total of 57,200 analyses, simply-supported beam-columns comprised of a fairly wide range of column W-sections and slenderness ratios are investigated for conditions of minor- or major-axis flexure that include or exclude the presence of residual stresses.

In general, all three elastic design methods provide fairly similar results, with AISC's relatively new Design by Advanced Elastic Analysis Method consistently indicating more strength (1% to 5%) than AISC's Effective Length and Direct Analysis design methods. Conditions of major-axis bending significantly improved the performance of all three elastic design methods. Regardless of the axis of bending, results are always improved when residual stresses are not present, a condition that is often the consequence of rotary straightening during the rolling process.

References

AISC (2016). *ANSI/AISC 360-16 Specification for Structural Steel Buildings*, American Institute of Steel Construction, Chicago, IL.

AISC (2016a). *Code of Standard Practice for Steel Buildings and Bridges*, American Institute of Steel Construction, Chicago, IL.

AISC (2016b). *Steel Construction Manual*, Fifteenth Edition, American Institute of Steel Construction, Chicago, IL.

Alemdar, B. N. (2001). *Distributed Plasticity Analysis of Steel Building Structural Systems.* PhD dissertation, Georgia Institute of Technology, Atlanta, GA.

Galambos, T.V. and Ketter, R.L. (1959), "Columns Under Combined Bending and Thrust", Journal of the Engineering Mechanics Division, ASCE, 85(EM2), pp. 135-152.

Ge, X. and Yura, J, (2019), "The Strength of Rotary-Straightened Steel Columns," Proceedings-Annual Stability Conference, SSRC, St. Louis, MO, pp. 425–442.

Giesen-Loo, E. (2016). *Design of Steel Structures by Advanced 2nd-Order Elastic Analysis –Background Studies*. Honors Thesis, Bucknell University, Lewisburg, PA.

Martinez-Garcia, J.M. and Ziemian, R.D. (2006), "Benchmark Studies to Compare Frame Stability Provisions," Proceedings-Annual Technical Session and Meeting, SSRC, San Antonio, TX, pp. 425–442.

McGuire, W., Gallagher, R., and Ziemian, R. (2000). *Matrix Structural Analysis*, John Wiley & Sons, Inc., New York, NY.

Nwe Nwe, M. T. (2014). *The Modified Direct Analysis Method: An Extension of the Direct Analysis Method*. Honors Thesis, Bucknell University, Lewisburg, PA

Appendices

A. Plots of interaction curves and percent radial errors

As a complement to Fig. 4, the remaining normalized *P-M* interaction curves and corresponding plots of percent radial errors that were studied for the specific case of a W12X50 member that includes residual stresses and subjected to minor-axis bending are provided.

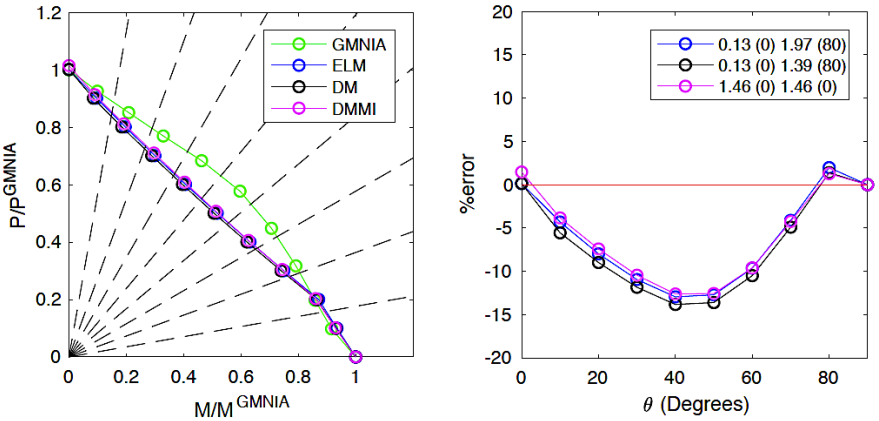

Figure A1: $L/r = 30$

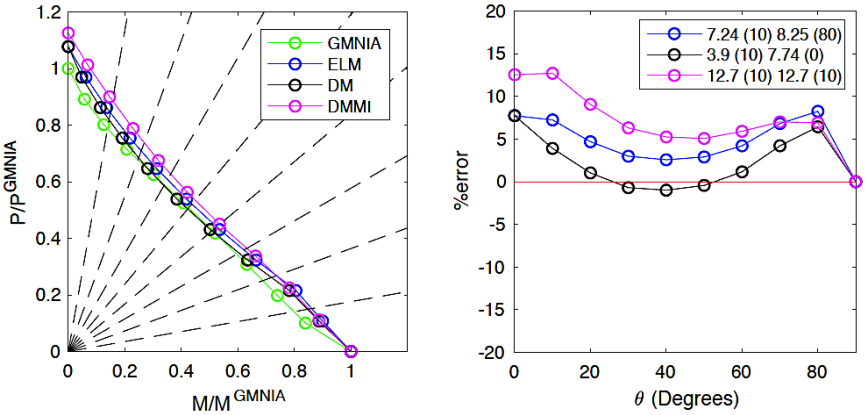

Figure A2: $L/r = 60$

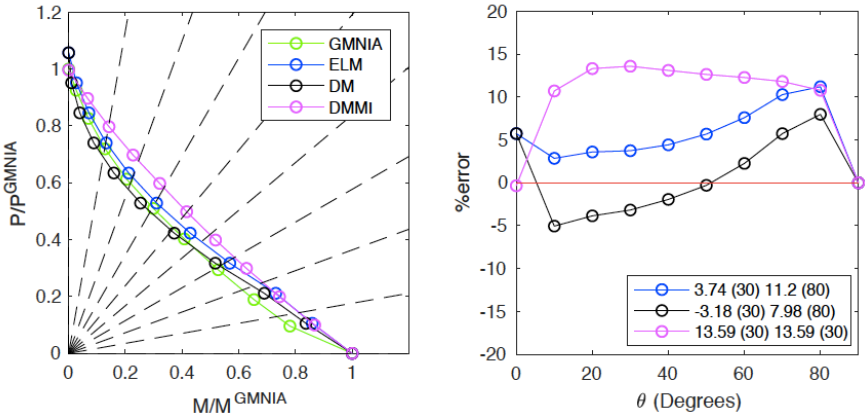

Figure A3: $L/r = 120$

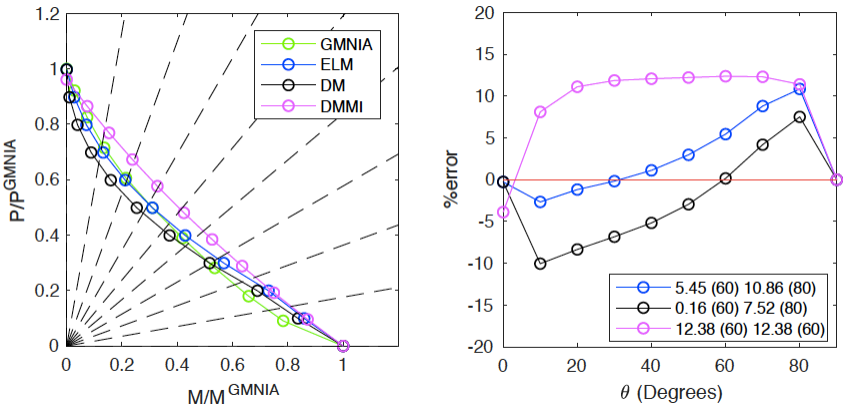

Figure A4: $L/r = 150$

B. Data for plots of percent radial errors

The following tables provide numerical values for the data points appearing in the percent radial error plots given in Fig. 4 and Appendix A.

Table B1: $L/r = 30$ (values are percent radial errors)

	Minor-axis bending with residual stresses			Minor-axis bending without residual stresses			Major-axis bending with residual stresses			Major-axis bending without residual stresses		
θ	DMMI	ELM	DM	DMMI	ELM	DM	DMMI	ELM	DM	DMMI	ELM	DM
0°	1.5	0.1	0.1	-6.2	-7.4	-7.4	1.9	-0.4	-0.4	-0.8	-3.1	-3.1
10°	-3.8	-4.3	-5.6	-7.2	-7.7	-8.9	3.5	2.3	0.9	-1.1	-2.2	-3.5
20°	-7.4	-8.0	-9.0	-9.1	-9.6	-10.6	4.7	3.4	2.3	-0.8	-2.0	-3.1
30°	-10.5	-11.0	-11.8	-12.1	-12.6	-13.5	5.2	4.1	3.1	1.2	0.1	-0.9
40°	-12.6	-13.0	-13.8	-14.5	-14.8	-15.7	5.4	4.6	3.5	4.2	3.3	2.3
50°	-12.6	-12.7	-13.6	-14.9	-15.1	-16.0	5.4	4.8	3.8	3.9	3.3	2.2
60°	-9.6	-9.6	-10.5	-12.2	-12.3	-13.2	5.2	4.9	3.9	5.0	4.7	3.6
70°	-4.3	-4.1	-4.9	-6.6	-6.5	-7.3	4.8	4.7	3.8	4.5	4.4	3.5
80°	1.3	2.0	1.4	0.3	1.1	0.5	1.6	2.2	1.6	2.2	2.8	2.2
90°	0.0	0.0	0.0	0.0	0.0	0.0	0.0	0.0	0.0	0.0	0.0	0.0

Table B2: $L/r = 60$ (values are percent radial errors)

	Minor-axis bending with residual stresses			Minor-axis bending without residual stresses			Major-axis bending with residual stresses			Major-axis bending without residual stresses		
θ	DMMI	ELM	DM	DMMI	ELM	DM	DMMI	ELM	DM	DMMI	ELM	DM
0°	12.5	7.7	7.7	-4.8	-8.8	-8.8	3.8	-2.6	-2.6	-6.6	-12.3	-12.3
10°	12.7	7.2	3.9	0.4	-4.5	-7.3	6.9	0.4	-2.7	-1.8	-7.8	-10.6
20°	9.1	4.7	1.0	0.0	-4.2	-7.5	8.1	2.5	-1.1	1.4	-4.0	-7.3
30°	6.3	3.0	-0.7	-1.5	-4.9	-8.3	8.5	4.0	0.3	3.4	-1.1	-4.6
40°	5.2	2.6	-1.0	-1.8	-4.6	-7.9	8.8	5.2	1.5	4.5	0.8	-2.8
50°	5.1	2.9	-0.4	-1.2	-3.4	-6.7	9.5	6.5	3.0	5.2	2.1	-1.4
60°	5.9	4.2	1.2	0.5	-1.3	-4.3	9.9	7.5	4.3	5.8	3.3	0.1
70°	7.0	6.8	4.2	3.4	2.5	-0.2	8.4	7.4	4.6	6.1	4.6	1.9
80°	6.9	8.3	6.4	5.5	7.0	5.0	4.4	5.6	3.7	2.9	4.1	2.1
90°	0.0	0.0	0.0	0.0	0.0	0.0	0.0	0.0	0.0	0.0	0.0	0.0

Table B3: $L/r = 90$ (values are percent radial errors)

	Minor-axis bending with residual stresses			Minor-axis bending without residual stresses			Major-axis bending with residual stresses			Major-axis bending without residual stresses		
θ	DMMI	ELM	DM	DMMI	ELM	DM	DMMI	ELM	DM	DMMI	ELM	DM
0°	8.2	9.4	9.4	-2.4	-1.3	-1.3	0.2	-1.2	-1.2	-6.5	-7.8	-7.8
10°	14.4	9.0	2.1	1.7	-3.0	-9.0	4.3	-1.9	-8.0	-1.0	-6.8	-12.5
20°	14.2	8.5	1.7	2.7	-2.5	-8.6	5.7	-0.6	-6.8	0.6	-5.5	-11.3
30°	13.1	7.6	1.3	3.1	-2.1	-7.8	6.9	0.7	-5.2	2.7	-3.3	-9.1
40°	12.4	7.2	1.3	3.9	-1.1	-6.7	8.0	2.2	-3.6	3.8	-1.9	-7.5
50°	12.3	7.5	2.1	5.5	0.9	-4.3	9.0	3.7	-1.7	4.0	-1.2	-6.4
60°	11.7	8.7	3.9	6.6	3.1	-1.6	9.0	5.0	0.2	4.6	0.4	-4.3
70°	11.2	11.2	7.1	7.3	6.6	2.4	7.5	6.4	2.2	4.3	2.8	-1.3
80°	9.9	11.4	8.5	8.1	9.7	6.7	4.4	5.7	2.8	2.0	3.3	0.4
90°	0.0	0.0	0.0	0.0	0.0	0.0	0.0	0.0	0.0	0.0	0.0	0.0

Table B4: $L/r = 120$ (values are percent radial errors)

	Minor-axis bending with residual stresses			Minor-axis bending without residual stresses			Major-axis bending with residual stresses			Major-axis bending without residual stresses		
θ	DMMI	ELM	DM	DMMI	ELM	DM	DMMI	ELM	DM	DMMI	ELM	DM
0°	-0.3	5.7	5.7	-6.4	-0.7	-0.7	-5.9	-1.7	-1.7	-6.7	-2.5	-2.5
10°	10.7	2.9	-5.0	0.4	-6.6	-13.7	0.9	-7.0	-14.1	-1.2	-9.0	-15.9
20°	13.3	3.6	-3.9	2.5	-6.2	-13.0	3.6	-5.9	-12.7	0.0	-9.2	-15.8
30°	13.6	3.7	-3.2	4.4	-4.8	-11.2	5.6	-4.4	-10.8	1.0	-8.6	-14.7
40°	13.1	4.4	-1.9	5.4	-2.9	-9.0	6.2	-2.8	-8.8	1.6	-7.1	-12.9
50°	12.6	5.7	-0.3	6.4	-0.4	-6.2	6.4	-1.0	-6.7	2.3	-4.9	-10.4
60°	12.3	7.6	2.3	7.5	2.6	-2.5	6.2	0.9	-4.2	2.2	-2.9	-7.8
70°	11.8	10.3	5.7	8.7	6.7	2.2	5.5	3.3	-1.1	1.9	-0.3	-4.5
80°	10.8	11.2	8.0	9.4	9.9	6.6	4.1	4.3	1.2	1.7	2.0	-1.1
90°	0.0	0.0	0.0	0.0	0.0	0.0	0.0	0.0	0.0	0.0	0.0	0.0

Table B5: $L/r = 150$ (values are percent radial errors)

	Minor-axis bending with residual stresses			Minor-axis bending without residual stresses			Major-axis bending with residual stresses			Major-axis bending without residual stresses		
θ	DMMI	ELM	DM	DMMI	ELM	DM	DMMI	ELM	DM	DMMI	ELM	DM
0°	-3.9	-0.3	-0.3	-5.8	-2.3	-2.3	-7.7	-5.3	-5.3	-9.2	-6.8	-6.8
10°	8.1	-2.7	-10.0	-0.6	-10.5	-17.3	-0.8	-11.3	-17.9	-4.9	-15.0	-21.4
20°	11.1	-1.2	-8.3	2.0	-9.2	-15.8	1.6	-10.3	-16.8	-1.9	-13.4	-19.6
30°	11.9	-0.2	-6.8	3.9	-7.4	-13.5	3.0	-8.8	-14.8	-0.1	-11.5	-17.4
40°	12.1	1.1	-5.2	5.4	-5.0	-10.9	3.9	-6.9	-12.8	0.5	-10.0	-15.7
50°	12.2	3.0	-2.9	6.9	-2.1	-7.7	4.5	-4.8	-10.3	0.1	-8.8	-14.1
60°	12.4	5.5	0.2	8.3	1.5	-3.6	4.8	-2.3	-7.4	0.5	-6.5	-11.3
70°	12.3	8.1	4.2	9.6	6.1	1.5	4.7	0.8	-3.6	0.9	-3.0	-7.2
80°	11.4	10.9	7.5	10.3	9.7	6.4	3.9	3.3	0.0	1.5	0.8	-2.3
90°	0.0	0.0	0.0	0.0	0.0	0.0	0.0	0.0	0.0	0.0	0.0	0.0